X Ray Imaging With a Silicon Microstrip Detector

Tadej Mali [1, 2], Vladimir Cindro [1] and Marko Mikuž [1, 2]
[1] Jožef Stefan Institute, Jamova 39, Ljubljana
[2] Department of Physics,University of Ljubljana, Jadranska 19, Ljubljana
e-mail: Name.Surname@ijs.si

Abstract

A small (3 mm wide) scanning test system was built and tested, using silicon microstrip detectors. Strips are oriented in parallel with the incident photon beam. High efficiency obtained in this way, depends mostly on the size of the guard ring. Images of simple objects were taken, contrast, detection limit and position resolution were studied.

1. Introduction

Breast cancer is a disease, which affects one out of 13 women in their life and one out of 25 dies because of it [1]. In order to cure the cancer effectively, an early and reliable diagnosis is essential. Therefore it is advisable for women over 50 years old to take regular X-ray examinations (mammography). However, exposure to X-ray radiation can provoke the disease itself. Therefore, it is necessary to minimize the delivered dose per mammographic examination. This can be achieved by using efficient, high resolution detectors for X-ray photons. One of the possibilities are. silicon microstrip detectors, which can have an efficiency in excess of 50%.

2. Imaging

2.1 Photon detection

In order to make a high contrast image, soft x-rays are used. Their energy ranges, depending on the tissue thickness, from 17 (2 cm of tissue) to 23 keV (8 cm of tissue) [2]. The mean free path of X-rays in silicon is between 0.60 mm (17 keV) and 1.6 mm (23 keV) [3], therefore the absorbing depth in the detector should be a few millimeters in order to efficiently absorb the incident photons.

A silicon microstrip detector is an array of thin, parallel, reverse biased p-n diodes. A traversing ionizing particle or photon generates electron-hole pairs in the depleted area. The generated charge is then collected and read out. The signal is directly proportional to the energy of incident photons and the average energy required to generate an electron-hole pair is 3.6 eV. Microstrip detectors are usually produced on thin (0.3 mm) silicon wafers and the length of strips is usually a few centimeters. If we orient the detector in such a way, that the incident photons hit the detector from the side (fig. 1), it acts as a pixel detector, where the size of the pixel is determined by the thickness of the wafer and the strip pitch. A 2D image can be obtained by scanning the object in the direction perpendicular to the detector plane.

The main source of noise in silicon microstrip detectors is the leakage current, which is caused by impurities or imperfections of the crystal lattice. Cutting the detector out of the wafer damages the crystal structure at the edges. This results in an increase of the leakage current [4]. Therefore the strips on the detector have to be kept away from the edge and a guard ring structure is inserted between strips and the edge of the detector. This represents a dead region of the detector, because the photons absorbed in the guard

ring can not be detected. The maximum efficiency of the detector is thus determined by the distance between the edge and the strips. For example, a detector with 0.30 mm wide guard ring and 22 keV incident photons, has an efficiency of about 80%.

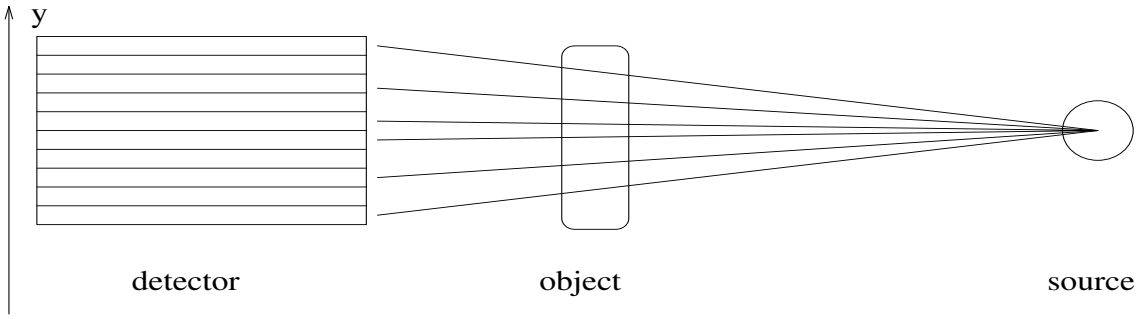

Figure 1: Imaging with silicon microstrip detectors.

2.2 Readout Electronics

X-ray imaging with silicon microstrip detectors is a single photon detection technique. Therefore an electronic system is required, which is capable of standalone multichannel, real-time, high-rate counting of current pulses, resulting from the hits of the photons on the pixels in the detector.

We have used a mixed analog-digital integrated circuit CASTOR[1] (**C**ounting and **A**mplifying **S**ys**T**em f**O**r **R**adiation detection) [5, 6, 7]. It is made in 1.2 μ VLSI technique [5] and optimised for the use in the Syrmep experiment [8]. Each channel consists of an analog part (charge sensitive preamplifier, shaper, filter) which is connected to a digital part (16-bit counter) via a comparator (only pulses, higher than the user-defined threshold, are counted); see fig. 2. The counting rate capability is limited by the analog part and it is about 100 kHz. After the acquisition the counters are connected into a shift register, the contents are read out and the IC is ready for the next acquisition.

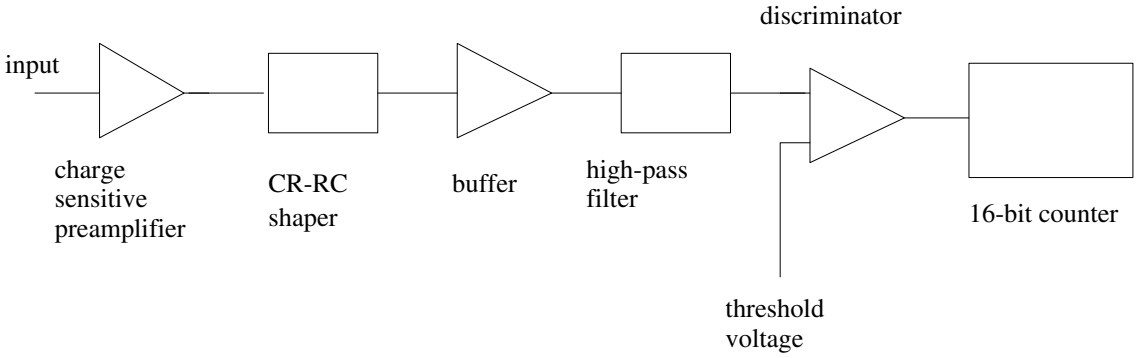

Figure 2: CASTOR block scheme.

We have measured the performance of the CASTOR circuit (gain, noise, counting rate) before mounting it to the detector.

In order to measure the gain (G) of the analog part, a series of voltage steps (ΔV) was applied to the capacitor (capacitance C_i) coupled to the input of preamplifier The number of detected pulses as a function of the threshold voltage. was measured and a counting curve obtained (fig. 3a). The response of the circuit is the threshold voltage, where half of the input pulses are counted. Using a 1.86 ± 0.04 pF capacitor, the calibra-

[1] CASTOR was developed by LEPSI, Strasbourg

tion curve for the analog part of the circuit was obtained (fig. 3b). It can be seen, that the response is linear for the input charge up to 2.5 fC (corresponding to approx. 55 keV photon). The gain (in the linear region) was determined to be $234 \pm 2 \pm 12$ mV / fC, where the first error is statistical and the second systematic. The gain of different channels is the same within 10%, and it slightly decreases with the input capacity (C_i): $G = \left((234 \pm 2) - (6.7 \pm 0.5) \times C_i \text{ / pF}\right)$ mV / fC. The errors are statistical, while the systematic errors are given by the error of the gain.

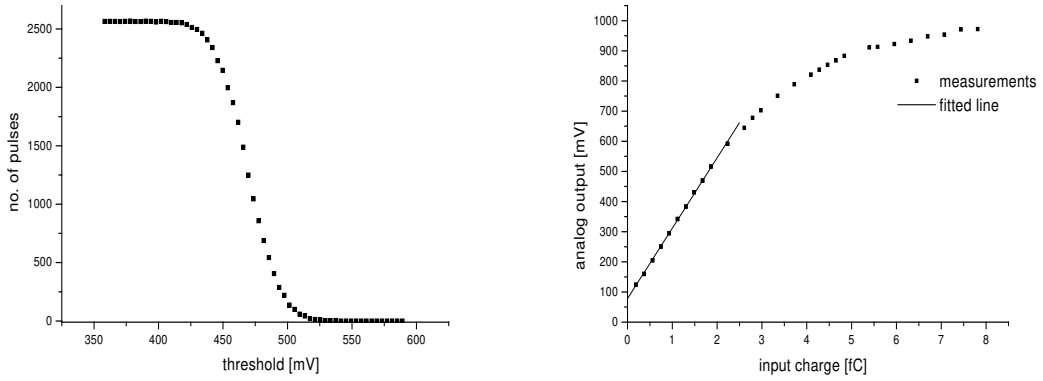

a) The counting curve b) The calibration curve of the analog part

Figure 3: Calibration of the analog part.

The noise was measured with the input capacitor grounded. Noise was determined by the standard deviation of a gaussian, which was fit on the derivative of the counting curve. Knowing the gain, the noise of the circuit can be expressed in *ENC* units. We found the noise to be: $ENC = (76 \pm 4 \pm 8)\ e_0 + (6.8 \pm 0.7 \pm 0.7) e_0 / \text{pF} \times C_i$; C_i is the stray capacitance at the input; the first error is statistical and the second systematic.

2.3 Detector

A silicon microstrip detector, which was made as a test structure for the development of the DELPHI spectrometer [9] at CERN was used. The detector was 0.3 mm thick with a strip pitch of 0.1 mm. Two neighbouring strips were bonded together, resulting in the pixel dimensions of 0.2×0.3 mm^2. The length of the strips was about 2 cm. The detector was cut 0.6 mm from the edge, giving an efficiency of 65% for 22.5 keV photons. The capacitance of a strip towards its neighbourhood was estimated to app. 3 pF.

The response of the detector connected to the readout electronics was tested, using a variable X-ray source. By changing the threshold voltage, the source spectrum was scanned. Since the energy of the photons is known, it was possible to determine the relation between the energy (E) of incident photons and the output of the analog part (V_{out}). The relation between V_{out} and E is: $V_{\text{out}} = (-75 \pm 3 \pm 4)$ mV $+ E \times (9.5 \pm 0.2 \pm 0.5)$ mV / keV; the first error is statistical and the second systematic.

2.4 Imaging System

The imaging system is shown on fig. 4. The detector and CASTOR are glued to a PCB, where the bias and control currents and voltages are filtered. The PCB is shielded by a metal box.

The control card consists of an analog and a digital part. The digital part is an interface between the computer and the IC; there is a level translator and a decoder, which

accepts the controls from the PC and generates the control signals for CASTOR. In the analog part of the control card there are biasing for the IC and control current/voltage sources for its analog part. There resides also a filtering system for the detector biasing.

The object under inspection was scanned using a moving stage. The stage can move the object in minimal steps of 0.0125 mm.

The source of X-rays was an X-ray tube with a tungsten anode, operating at 25 kV anode voltage.

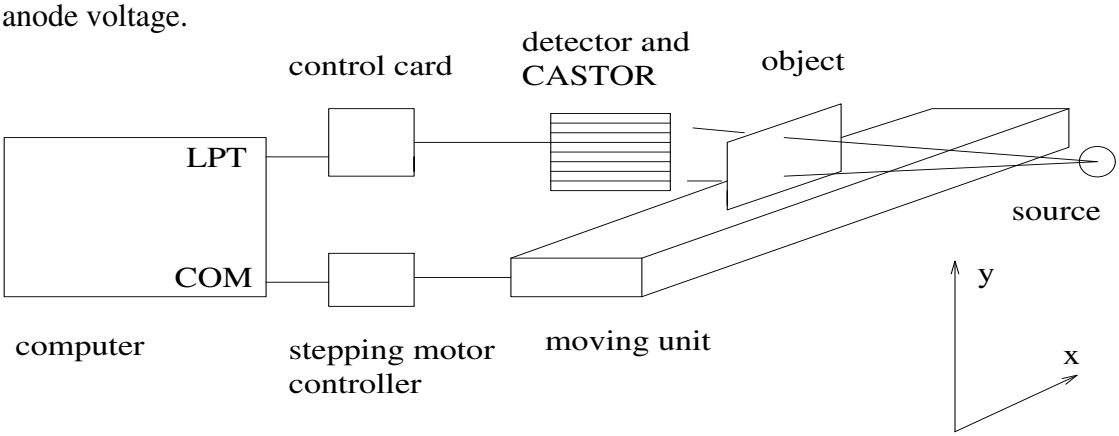

Figure 4: Imaging system.

2.5 Images and Analysis

In X-ray imaging it is essential to distinguish small objects embedded in a tissue. This is possible because of different attenuation properties of the inspected tissues. We define the contrast (C) as [2]:

$$C = \frac{|N_1 - N_2|}{N_1}, \tag{1}$$

where N_1 is the number of photons per pixel in the area, with tissue only (background), while N_2 is the number of photons per pixel in the area, where they pass the object. The signal (S), that we are interested in, is the difference between detected photons in the background and in the area, where the object resides:

$$S = |N_1 - N_2| = CN_1. \tag{2}$$

Because of fluctuations in the background (noise), the signal must be significantly higher than the noise. The working condition for the signal to noise ratio (SNR) requires it to be above 5 to clearly see the object. As the noise increases as $\sqrt{N_1}$, SNR increases as:

$$SNR = \frac{|N_1 - N_2|}{\sqrt{N_1}} = C\sqrt{N_1} \propto \sqrt{\text{dose}} \tag{3}$$

Therefore, objects cannot be seen until the delivered dose is high enough for the SNR to be above 5.

The described system was used to make images of simple objects - a thin (0.1 mm) Al foil, with small holes through it (fig. 5). The object contrast is approx. 0.07 and it corresponds to a microcalcification with a diameter of 0.05 mm in woman's breast. The diameters of the holes are: (upper row, from left to right) 2×0.25 mm (two holes, which cannot be distinguished and appear as a single one), 0.40, 0.50, 0.58, 0.65, 0.80 and 0.90 mm. There is also a hole in the lower left corner; its diameter is 0.25 mm.

The effect of increasing the dose can be seen in fig. 5. The noise of the background was calculated as the rms of the number of detected photons in the vicinity of the holes and the signal was calculated as the difference between the number of detected photons

in the background and the number the maximum number of photon counts in a pixel in the signal region.

The image contrast was calculated as a relative difference between signal and background (eq. 1) and the values obtained ranged between 0.06 (0.80 mm hole) and 0.01 (0.25 mm hole), depending on the size of the object.. The contrast is in good agreement with that expected for big objects and is lower for objects comparable or smaller than the pixel size. This can be explained by signal sharing between the neighbouring pixels.

The obtained *SNR* was plotted and fitted by a square root function (fig. 6, next page). Considering the requirement *SNR*=5, the required dose per investigation could be calculated [10]. The results are summarised in table 1. Low contrast objects require higher dose, as predicted in eq. 3.

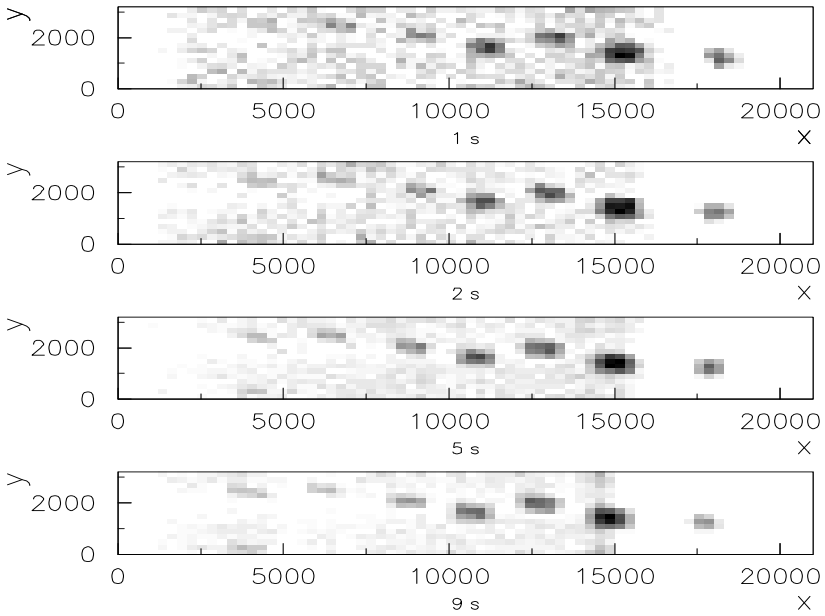

Figure 5: Images of a simple object, taken at different exposure times (1s to 9s). The exposure time of 1 s equals approx. 40000 detected photons per pixel in the background. The measured contrast in the picture is between 0.01 and 0.06.

tissue thickness [cm]	photon energy [keV]	2*r*=0.5 mm dose [mGy]	2*r*=0.25 mm dose [mGy]
2	17	1.2/η	8/η
4	20	1.8/η	13/η
6	22.5	2.0/η	14/η
8	23	5.4/η	39/η

Table 1: Estimation of the superficial dose per investigation, required to see an object with the given diameter and contrast of 0.07 (η is the efficiency of the detector).

3. Conclusions

The first tests of the system were successful. The performance of the readout electronics is in good agreement with manufacturer's specifications.

The measurements with a thin Al foil (0.1 mm) showed, that low contrast objects (*C*=0.07) with a diameter of 0.5 mm, embedded in 4 cm thick tissue could be seen with a superficial dose of 2.8 mGy per investigation, using a detector with 65% efficiency.

Further improvements in spatial resolution and image processing would significantly improve the detectability of objects. Together with higher efficiency of the detector (reduced dead region) this would also contribute to a lower superficial dose.

To obtain an objective comparison between the conventional method (film) and the new technique (silicon microstrip detectors), a test of our system with a conventional mammographic phantom is planned.

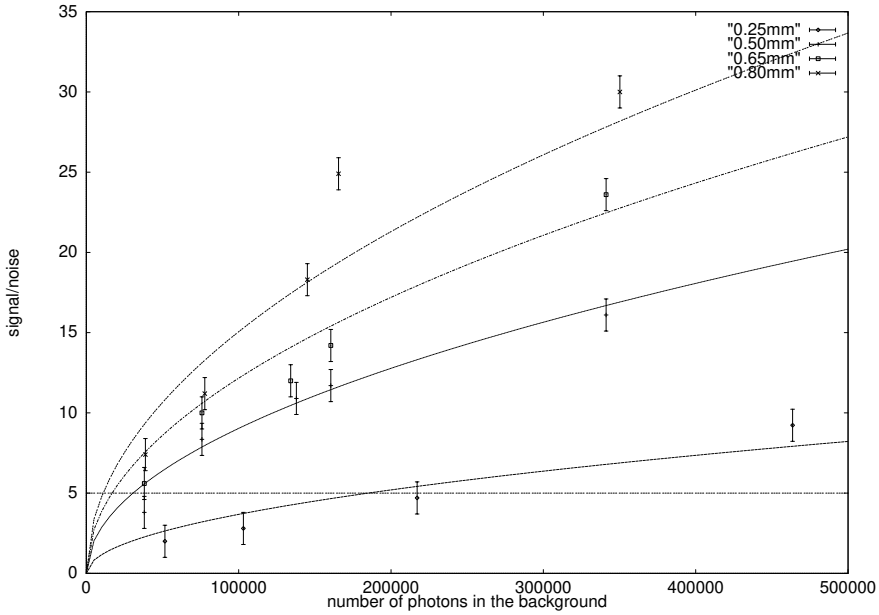

Figure 6: *SNR* as a function of number of detected photons in the background.

4. References

[1] G. Stafford, *Mammography Basic Principles*, American Medical Association, Chicago, 1992

[2] W. Swindell, S. Webb, *The Physics of Medical Imaging*, IOP Bristol and Philadelphia, 1992

[3] Mucal on The Web, http://www.csri.iit.edu/mucal.html

[4] F. Arfelli et. al., Developments in the field of silicon detectors for digital radiology, , *Nuclear Instruments and Methods* A377, 1996, 508-513

[5] G. Comes et. al. CASTOR a VLSI CMOS Mixed Analog-Digital Circuit for Low Noise Multichannel Counting Applications, *Nuclear Instruments and Methods* A377, 1996, 440-445

[6] CASTOR 0.0, User Manual, 1995

[7] CASTOR 1.0, User Manual, 1996

[8] F. Arfelli et. al., Silicon Detectors for Synchrotron Radiation Digital Mammography, *Nuclear Instruments and Methods* A353, 1994, 366-370

[9] V. Cindro et. al., The design of silicon ministrip detectors for the DELPHI Very Forward Tracker, *Nuclear Physics* B44, 1995, 292-295

[10] T. Mali, Postavitev sistema za rentgensko slikanje s silicijevimi mikropasovnimi detektorji, Diplomsko delo, Oddelek za fiziko, Univerza v Ljubljani, 1997.